
Article:
Michie, EAH, Yielding, G and Fisher, QJ orcid.org/0000-0002-2881-7018 (2018) Predicting Transmissibilities of Carbonate-hosted Fault Zones. Geological Society Special Publications, 459 (1). pp. 121-137. ISSN 0305-8719

https://doi.org/10.1144/SP459.9

Predicting Transmissibilities of Carbonate-hosted Fault Zones

E. A. H. Michie [1]*, G. Yielding[1] & Q. J. Fisher[2]

[1] Badley Geoscience Ltd, North Beck House, North Beck Lane, Hundleby, Spilsby, Lincolnshire, PE23 5NB

[2] School of Earth and Environment, University of Leeds, Leeds, LS2 9JT

***Corresponding author:** emma@badleys.co.uk

Keywords: fault rock; carbonates; microstructures; normal faults; hydraulic behaviour; transmissibility; geomodelling

Abbreviated title: Transmissibilities of Faulted Carbonates

Abstract

It is common practice to incorporate deterministic transmissibility multipliers into simulation models of siliciclastic reservoirs to take into account the impact of faults on fluid flow, but this not common practice in carbonate reservoirs due to the lack of data on fault permeability. Calculation of fault transmissibilities in carbonates is also complicated by the variety of mechanisms active during faulting, associated with their high heterogeneity and increased tendency to react with fluids. Analysis of the main controls on fault rock formation and permeability from several carbonate-hosted fault zones is used to enhance our ability to predict fault transmissibility. Lithological heterogeneity in a faulted carbonate succession leads to a variety of deformation and/or diagenetic mechanisms, generating several fault rock types. Although each fault rock type has widely varying permeabilities, trends can be observed dependent on host lithofacies, juxtaposition and displacement. These trends can be used as preliminary predictive tools when considering fluid flow across carbonate fault zones. At lower displacements (<30 m), fewer mechanisms occur, creating limited fault rock types with a narrow range of low permeabilities, regardless of lithofacies juxtaposition. At increased displacements, more fault rock types are produced at juxtaposition of different lithofacies, with a wide range of permeabilities.

Although the influence of faulting on fluid flow pathways in carbonate reservoirs often receives significant attention, there is surprisingly little data published on the wide variety of microstructures that can occur in carbonate fault cores, the controls on the variation, and linking of microstructures to measured porosity and permeability, which could be used to predict their impact on fluid flow (e.g. Tondi *et al.* 2006; Agosta 2008; Bastesen *et al.* 2009). The sealing potential of faults in siliciclastic sequences, on the other hand, has been widely documented (e.g. Knipe 1992; Antonellini and Aydin 1994; Caine *et al.* 1996; Evans *et al.* 1997; Fulljames *et al.* 1997; Knipe 1997; Yielding *et al.* 1997; Fisher and Knipe 1998, 2001; Crawford *et al.* 2002; Flodin *et al.* 2005; Færseth *et al.* 2007; Yielding 2015). It is considered that within a sand-shale sequence containing a high proportion of shale, faults have a high potential for clay smear or gouge to be generated, lowering the permeability to create a baffle / seal (Yielding *et al.* 1997; Fisher and Knipe 1998). This premise is used when calculating transmissibility multipliers that may be incorporated into simulation models of siliciclastic reservoirs to take into account the impact of faults on cross formational fluid flow. While faulted carbonate sequences with shaley intervals may allow for the use of algorithms currently in place, such as the shale gouge ratio or shale smear factor, in faulted carbonates that lack shaley interbeds, algorithms such as the shale gouge ratio cannot be applied, and no other algorithms exist to predict their sealing potential. Ultimately this also means there is no equivalent methodology to predict fault transmissibility multipliers for carbonate-dominated reservoirs.

The high degree of alteration and heterogeneity of carbonates (e.g. Lucia *et al.* 2003; Tucker and Wright 2009; van der Land *et al.* 2013) often leads to the assumption of a

heterogeneous fault core. Also, the chemical reactivity of carbonates means that they often experience more rapid porosity loss during burial than siliciclastics (e.g. Erhenberg and Nadeau, 2003). This simplified view of carbonate diagenesis has led to the overall assumption that carbonates will deform in a brittle manner resulting in the formation of flow conduits instead of barriers. However, the present study shows that a variety of brittle and ductile deformation mechanisms occurs in carbonate faults on Malta, and patterns of fault core heterogeneity can be observed and used to attempt to predict their hydraulic behaviour.

Faulted carbonates have been documented as having a range of sealing potential, from barriers (Giurgea *et al.* 2004) to conduits (Billi *et al.* 2007), or dual conduit-seal characters (Agosta 2008). It has been shown in siliciclastics that the deformation style varies with protolith porosity (Groshong 1988; Shipton and Cowie 2003); high porosity rocks tend to cataclase, whereas low porosity rocks tend to fracture. Similar results have also been documented in carbonate lithofacies, but with added complexities. For example, carbonates with high initial porosities can deform locally, by particulate flow and pressure solution to produce shear bands that lower the porosity (Tondi 2007), as well as cataclastic flow that produces protocataclasite and cataclasite fault rocks (Micarelli *et al.* 2006). Further, carbonates with lower initial porosities have also been documented as deforming by cataclasis, and diagenetically altering by cementation, which can also lower the porosity of the fault rock (Agosta *et al.* 2003; Agosta 2008). Fracturing, however, can be prevalent within carbonates, causing an increase in permeability (Billi *et al.* 2007). The heterogeneous nature of carbonates, high diagenetic potential and wide range of textures and pore types in

carbonates with similar porosities can cause complexities to the fault rock types produced, resulting in many fault rock types (Bastesen *et al.* 2009; Bastesen and Braathen 2010; Michie 2015), all of which could have different permeabilities (Michie and Haines 2016).

There are a range of methods available to calculate transmissibility multipliers that may be incorporated into simulation models of siliciclastic reservoirs to take into account the impact of faults on fluid flow; these tend to be based on estimated fault thickness and the clay content of the fault rock. For example, the documented and widely used equations of Manzocchi *et al.* (1999) depend on fault rock thickness, fault rock permeability and surrounding cell permeabilities and sizes. The model for fault rock thickness uses a linear relationship defined between fault displacement and fault rock thickness, based on outcrop data (e.g. Hull 1988; Knott *et al.* 1996; Foxford *et al.* 1998; Walsh *et al.* 1998). Fault rock permeability can be calculated using estimates of the fault rock composition using algorithms such as the shale gouge ratio (Yielding *et al.* 1997), which calculates the amount of shale entrained into the fault using a relationship between VShale / VClay and throw. There is, however, no equivalent methodology to predict fault transmissibility multipliers for shale-poor carbonate reservoirs. Since the equations to calculate transmissibility and transmissibility multipliers are reliant on the VShale of a sequence, and although some sequences do contain shale layers resulting in the formation of a shale smear (e.g. Aydin and Eyal 2002), a question could be asked about the applicability of these equations to calculate the transmissibility of faults cutting a sequence of pure carbonates. In particular, many carbonates lack any shale component and hence do not produce clay-rich fault rocks.

This preliminary study attempts to calculate fault transmissibility using patterns observed in outcrop data from Malta that have shown how fault rock types, and hence their permeability, vary according to host lithofacies, displacement and juxtaposition (Michie 2015; Michie & Haines 2016). These calculations of fault transmissibility can only currently be applied to Malta, with the ultimate aim to expand the calculation to allow application to different carbonate sequences, through continued research. Although severe heterogeneity is recorded in these carbonate fault rocks, patterns to this variability have been recorded and can be used to predict the fault rock permeability on Malta under different scenarios. This study documents the porosity and permeability of several fault rock types to increase our understanding of the main controls on the fault's hydraulic behaviour, which are then used to calculate transmissibility multipliers of carbonate-hosted faults on Malta to improve simulation of flow in analogous carbonate reservoirs. This study signifies the start of a database collating carbonate fault rock porosity and permeability through ongoing research, with the ultimate aim of creating a more generalised algorithm to predict fault transmissibility multipliers of faulted carbonates.

Geological Setting

The dataset used in this study is based on outcrop samples from the island of Malta. Malta was chosen as the initial locality because of its tectonic simplicity, minimal background diagenesis and faults that range in displacement and cut through varying lithofacies. The faults in this study have gone through one main tectonic phase of extension during the Pliocene to Quaternary, associated with approximately N-S stretching within the foreland of

119 the Sicilian Apennine-Maghrebian fold-thrust belt that created a conjugate rift system: the
120 ENE-WSW trending Maltese graben system and the NW-SE trending Pantelleria rift system
121 (Pedley *et al.* 1976; Dart *et al.* 1993; Fig 1). The focus of this study has been on the ENE-
122 WSW trending faults of the North Malta Graben that range in displacement from as little as
123 10 cm up to 90 m (Fig. 1). These faults have gone through only one phase of burial
124 (shallowly buried to roughly 300 m, see Bonson *et al.* 2007), followed by uplift.

125 The faults examined in this study displace lithofacies that vary from fine-grained mud-
126 wackestone to packstones and boundstones (Fig. 1). These faults cut two main exposed
127 formations: the Lower Coralline Limestone Formation (LCL), a coarse-grained, bioclastic-rich
128 limestone, which is overlain by the fine-grained carbonate dominated by *Globigerina*
129 foraminifera with sparse macro-fossils, known as the Globigerina Limestone Formation (GL)
130 (Pedley *et al.* 1976; Dart *et al.* 1993; Fig. 1). For the sake of simplicity, these two formations
131 (LCL and GL) are considered as grain- and micrite-dominated carbonates respectively,
132 associated with their corresponding textures and deformation styles.

133 Grain-dominated carbonates are coarse, grain-supported, containing macro (>250 μm) fossil
134 clasts, and minor micritic matrix (Fig. 2), with a Uniaxial Compressive Strength (UCS) of *c.*80
135 MPa, determined from Schmidt Hammer measurements (Michie *et al.* 2014). This
136 lithofacies is usually composed of packstones and boundstones. The micrite-dominated
137 carbonate is a micritic-rich lithofacies, supporting micro fossils (<50 μm), and occasionally
138 contains dispersed large >250 μm bioclasts (Fig. 2). This lithofacies is primarily composed of
139 wackestones and has a UCS of *c.*40 MPa (Michie *et al.* 2014). The majority of the LCL is
140 grain-dominated; however some beds within the Il Mara Member at the top of the LCL are

micrite-dominated (Fig. 1). The Lower *Globigerina* Limestone (LGL) and Middle *Globigerina* Limestone (MGL) members of the GL are both micrite-dominated carbonates (Fig. 1). Both lithofacies (grain- and micrite-dominated carbonates) have a high, *c.*30%, porosity, but with variable permeabilities. The strong grain-dominated carbonates have an average permeability of *c.*200 mD, whereas the weaker micrite-dominated carbonates have a much lower average permeability of *c.*2 mD (Fig. 2).

The fault zones studied have an added complex architectural component (the Fracture Splay Zone), observed solely within the micrite-dominated carbonates, associated with the mechanical stratigraphy created by the stronger (c.80 MPa UCS) carbonates (grain-dominated carbonates) overlain by the weaker (c.40 MPa UCS) carbonates (micrite-dominated carbonates) (Michie *et al.* 2014). The Fracture Splay Zone (FSZ) is an area of intensely fractured rock, containing and bound by slip surfaces. When micrite-dominated carbonates are juxtaposed against grain-dominated carbonates, a point of high strain is produced from which subsequent slip surfaces propagate out and upwards to follow the fault trend. This architecture occurs in all fault zones with displacement over 1 m, where sufficient mechanical contrast occurs after juxtaposition (Fig. 3). Surrounding the FSZ is a zone of weaker deformation (fracturing), which terminates in the protolith. Conversely, when faulting juxtaposes the stronger grain-dominated carbonates next to itself, propagation of further slip surfaces does not occur; instead deformation localises around a single principal slip surface creating a narrow zone of symmetrical damage which exponentially decreases into the protolith. This fault zone architecture conforms to that described originally by Chester and Logan (1986).

Fault zone architectures have significant effect on the distribution of fault core; multiple slip surfaces that form the FSZ cause fault core production to be distributed across the fault zone (Fig. 3), such that a continuous fault core is not observed at lower displacements (<30 m). Although fault rock can be observed as relatively small discontinuous pods on several slip surfaces within the FSZ with individual displacements of >0.5 m, fault core is mainly observed on the principal slip surface with the most accumulated displacement (Michie *et al.* 2014).

Methods

Examination of how fault rocks vary between two lithofacies with increasing displacement advances our understanding of the main controls on the deformation style, and hence fault rock production and evolution, including permeability. Since the faults in the studied sequence juxtapose two different carbonate lithofacies, with varying textures, strength and permeabilities, but with similar porosities, this has allowed analysis of what ultimately controls fault rock production and their respective permeabilities.

Field mapping

Two areas on Malta have been studied in detail: the Ras ir Raheb coastal section and Madliena Tower (Fig. 1; see Michie *et al.* 2014; Michie 2015 for more detail). Fault zones that vary in displacement from 0.52 m to 25 m have been mapped at Ras ir Raheb. These maps detail the location, geometries and type of fault rock within the fault core, at a scale of

184 1:100. Madliena Tower exposes the Victoria Lines Fault (VLF) with a *c.*90 m displacement
185 fault zone, and *c.*60 m on the principal slip surface (90 m value from House *et al.* 1961).
186 Maps have been constructed at a scale of 1:250, which also record the location, geometry
187 and types of fault rock (see Michie *et al.* 2014 for map examples).

188

189 **Microstructural analysis**

190 Deformation microstructures of eighty-seven oriented fault rock samples from fault zones of
191 varying displacement up to 90 m have been examined using optical thin section and
192 Scanning Electron Microscope – Back-scatter Electron microscopy (SEM-BSE) to document
193 the dominant microstructural textures. The deformation mechanisms for each lithofacies
194 have been inferred from the recorded microstructures. Deformation mechanisms
195 documented range from elastic-frictional to crystal-plastic deformation, and have been used
196 to create a classification for these fault rocks in the two carbonate lithofacies on Malta
197 (Michie 2015).

198

199 **Porosity and permeability measurements**

200 Porosity and permeability measurements were made on 69 1" diameter core plugs drilled
201 from fault core samples containing 100% volume of fault rock, with as much surface
202 weathering removed as possible. Each thin section was taken close to, and with the same
203 orientation as, the core plugs in order to specify the porosity and permeability of each fault
204 rock type defined by observed microstructures. Hence, the thin sections represent the

205 microstructures within the core plugs. The range of porosity and permeability defined for
206 each fault rock type is used to infer the controls on the hydraulic behaviour of carbonate
207 fault zones. Specifically, the inferred diagenetic and/or deformation mechanisms creating
208 each fault rock type can be analysed as increasing or decreasing porosity and/or
209 permeability, and to what extent.

210 Porosity was calculated by subtracting the grain volume from the bulk volume, which used
211 measured core plug dimensions. Grain volume was measured on dry cores at ambient
212 stresses using a Coberly-Stevens helium porosimeter, which is a double-cell method based
213 on Boyle's law. Measurements of each fault rock sample were repeated a minimum of 3
214 times to check the accuracy and decrease the standard deviation of the measurements to
215 2%. The average was then taken from the ≥3 measurements after any anomalous results
216 (±2%) have been removed.

217 Steady state permeability was measured using a Jones nitrogen permeameter, on dry cores
218 at ambient pressures and at room temperature. The core plug was placed within a Hassler
219 sleeve and a confining pressure of 400 psi was applied. Five nitrogen gas pressures were
220 added (up to 60 psi) and the flow readings recorded for each pressure. These flow readings
221 were used to calculate the permeability using Darcy's law. This permeability is corrected for
222 gas slippage using the Klinkenberg method with 5 individually measured points creating a
223 linear regression of an inverse pressure with permeability (Klinkenberg 1941). While the
224 permeability measured using the Mariam oil manometer is accurate only down to *c.*0.5mD,
225 the use of a travelling meniscus means that this method can accurately measure
226 permeabilities as low as 0.0001 mD, by measuring flow rates down to 0.00001 ml/s^{-1}.

However, it is acknowledged that permeabilities nearing 0.0001 mD are unlikely to be as accurate as values above this.

Calculating Transmissibilities and transmissibility multipliers

A reservoir model (from Manzocchi *et al.* 1999) spanning 60 x 20 x 20 (x, y, z) cells and a cell size of 150 x 180 x 10 m, has been used to analyse the impact of lithofacies variation, specifically petrophysical properties, on fault permeability and hence fault transmissibility. Two faults from the model have been selected for detailed examination, as these have similar throws to those analysed in the field; one with 15 m throw and another with 60 m throw. Cells in this reservoir model in the TransGen module of TrapTester-T7 software were populated with porosity and permeability using a simple deterministic method, assuming the cell property varies continuously across the grid, using well picks as layer boundaries. The layers in the model were populated according to the properties in an upscaled representation of the logged stratigraphic sequence of Malta (Fig. 1 and 2C) using a synthetic log (see logs on Figs. 7 and 8). This upscaling method arithmetically averages porosity values and geometrically averages permeability values from the synthetic log.

Transmissibilities and transmissibility multipliers have been calculated manually and in TrapTester-T7 using equations from Manzocchi *et al.* (1999), equation (1), with permeabilities based on observed host and fault rock permeabilities associated with specific controls, namely, host lithofacies, displacement and juxtaposition types.

$$T = [1 + t_f \frac{\left(\frac{2}{k_f} - \frac{1}{k_i} - \frac{1}{k_j}\right)}{\left(\frac{L_i}{k_i} + \frac{L_j}{k_j}\right)}]^{-1} \quad (1)$$

where T is the transmissibility multiplier to capture the effects of fault rock between cells, tf is the fault rock thickness that has been harmonically averaged, kf is the permeability of the fault rock, arithmetically averaged, ki and kj are the permeability of the surrounding cells, and Li and Lj are the lengths of the surrounding cells. See Manzocchi *et al*. (1999) for more detail.

To predict any potential flow across fault zones, a model is required for upscaling core plug permeability measurements and fault rock thickness measurements to sub-cellular components, which are then upscaled further to populate a cell connection with a single uniform transmissibility value. Permeability heterogeneity at the sub-metre scale has been upscaled to sub-cell components using the geometric average of individually measured fault rock permeabilities (Fig. 4, black arrows). This scale of heterogeneity can include variations of permeability within a single fault rock sample and variations of fault rock type (and hence permeability) perpendicular to fault strike. The geometric averaging has been chosen as this provides more meaningful averages to permeability values with a large range (often over 4 orders of magnitude for permeability can occur in a single fault rock sample). To upscale the sub-cell components to a cellular grid and generate a uniform transmissibility at cell connections, the area-weighted (A) arithmetic mean of the sub-cell fault rock permeability (kf) is taken to keep the pressure drop constant across the fault (equation 2, Fig, 3; see Manzocchi *et al.* 1999 for more detail).

$$k_f = \frac{1}{A}\sum_{i=1}^{i=n} k_{fi}A_i \quad (2)$$

Fault rock thickness heterogeneity at the sub-metre scale has been upscaled using the arithmetic average, due to the low range in values per sample (Fig. 4, red arows). To upscale the sub-cell thickness variations to the cell size and generate transmissibilities at cell connections, the area-weighted (A) harmonic average of each fault rock thickness (tf) is taken to keep the pressure drop constant across the fault (equation 3, Fig 3; see Manzocchi *et al.* 1999 for more detail).

$$t_f = A\left[\sum_{i=1}^{i=n} \frac{A_i}{t_{fi}}\right]^{-1} \quad (3)$$

Fault rock types and their petrophysical properties

Previously documented microstructural and petrophysical data (Michie 2015; Michie & Haines 2016) is summarized below before the method to incorporate these data into transmissibility multipliers is described.

Nine different types of fault rocks are observed within the fault zones on Malta, and these vary according to the host lithofacies. Although previous studies suggest that porosity has a principal control on deformation style (Groshong 1988; Shipton and Cowie 2003), the range of fault rock types occurring on Malta varies between two carbonate lithofacies with similar, high porosities (Michie 2015). Hence, the protolith texture, rather than porosity alone, has a major impact on deformation style and therefore fault rock type and properties. Not only does the type of fault rock and its permeability vary with displacement, as shown in

previous studies (e.g. Antonellini and Mollema 2000), but the abundance and location of each fault rock type are also heavily dependent on lithofacies juxtaposition.

Micrite-dominated carbonates

Micrite-dominated carbonates deform by dispersed mechanisms, specifically through-going fractures, associated with their homogeneous, fine-grained texture dominated by microporosity, creating low/no mechanical discontinuities to prevent fracture propagation and cause restriction to fossil clasts (Kranz 1983; Groshong 1988). These fractures coalesce to produce a variety of dilation breccias with added complexities such as polyphase brecciation, recrystallisation, dissolution and fracture overprinting (Michie 2015; Fig. 5). In areas away from these fractures and breccias, the matrix shows well-defined crystals with wavy grain boundaries that overprint the original texture (Fig. 5), occlude the pre-existing pore spaces and show a strong crystallographic preferred orientation (CPO). These are recrystallised fault rocks that formed from *e* twinning (Michie 2015).

Grain-dominated carbonates

Grain-dominated carbonates deform by grain-scale mechanisms, specifically cataclasis, associated with clast-confined fractures forming due to their heterogeneous, coarse-grained textures, with a wide variety of pore types, such as vuggy, intra and intergranular pores (Michie 2015). These intragranular cracks increase in intensity and evolve to create protocataclasites and cataclasites, which can later fracture and brecciate to create

308 composite chaotic breccias (Fig. 5). Alternatively, this lithofacies is also observed to have
309 limited deformation; instead they can diagenetically alter, specifically by aggrading
310 neomorphism transforming micritic matrix into sparite, infilling pores (Michie 2015; Fig. 5).

311

312 **Porosity and permeability trends**

313 Although each fault rock type has variable petrophysical properties, causing the
314 permeability to vary from 0.0001 mD to over 1000 mD (see Michie & Haines 2016; Fig. 6A),
315 there are patterns to the variation in permeability, which can be used predictively. Figure
316 6B, C and D illustrate the variation of fault rock permeability with displacement, host
317 lithofacies and juxtaposition type, respectively. In Figure 6B, the distribution of individual
318 data-points is shown at the appropriate displacement value, and the distribution is
319 summarized as a frequency histogram (horizontal bars) and a frequency curve. The
320 histograms have not been plotted on Figures 6C and D for the sake of clarity.

321 The permeability of fault rocks is often recorded as being lower than their respective host
322 rock; however, there are measured occurrences where fault rocks either have the same or
323 higher permeabilities (Fig. 6). Where the higher / lower permeability fault rock occurs is
324 highly dependent on both the displacement and the lithofacies juxtaposition type.

325

326 *Displacement and Lithofacies Controls on Fault Rock Permeability*

327 Fewer fault rock types are observed at lower displacements (<30 m) when compared with
328 higher displacement fault zones, which acts to reduce the range of permeability. Moreover,

329 the majority of fault rocks at lower displacement have low permeabilities (Fig. 6B). At low
330 displacements, micrite-dominated fault rocks are only produced when micrite-micrite
331 juxtapositions occur, and these fault rocks are restricted mainly to recrystallised fault rock
332 types. The limited range of fault rock types in this scenario creates a low range of
333 permeability with values reduced from the host rock (Fig. 6C, red curve). Grain-dominated
334 fault rocks are produced at both grain-grain and grain-micrite juxtapositions at low
335 displacements, creating two different fault rock types; mainly protocataclasite and
336 composite chaotic breccias (Michie 2015). While these fault rocks can have a relatively large
337 permeability range, there is a greater occurrence of lower permeability fault rocks (Figs. 6C,
338 blue curve).

339 At displacements >30 m a larger range of permeability is observed than at lower
340 displacements, <30 m (Fig. 6B). Micrite-dominated fault rocks can be produced at both
341 micrite-micrite and micrite-grain juxtapositions at higher displacement, causing their
342 permeability range and average value to increase with displacement (Fig. 6C).

343

344 *Juxtaposition types*

345 Although displacement and host lithofacies can be used to determine fault rock
346 permeability ranges and average values to improve predictability of a fault's transmissibility,
347 these controls can be further advanced by distinguishing permeabilities at certain lithofacies
348 juxtaposition types.

Fewer fault rocks types are observed when similar lithofacies are juxtaposed, at both low and high displacements, with a narrow measured permeability range and overall low permeability (Fig. 6D, red and blue curves). These areas could, therefore, potentially reduce across fault flow. For example, recrystallised fault rocks are common, along with occasional mosaic or chaotic breccias, when micrite-dominated carbonates are self-juxtaposed (Michie 2015), which creates a narrow range of low permeability. When grain-dominated carbonates are self-juxtaposed, grain-scale deformation occurs, creating protocataclasites, cataclasites or composite chaotic breccias. Alternatively, grain-dominated fault rock can be cemented without significant deformation. Although the range of permeability at grain-grain juxtapositions is large, the majority of these fault rocks have low permeabilities (Fig. 6D, blue curves). However, when different lithofacies are juxtaposed, a high heterogeneity of fault rock types is observed, along with a high range in permeability, and a high average permeability value (Michie and Haines 2016). This is particularly evident at higher displacements along the principal slip surface where grain-micrite juxtaposition occurs, with a continuous fault core containing a mixture of micrite- and grain-dominated carbonate fault rock. These fault rock types include: cataclased, brecciated (different types), cemented and recrystallised, all with significantly varying permeabilities (Fig. 6D, green curve at high displacement). Hence, under these conditions, the fault may be more transmissive. Conversely, fewer fault rock types, dominated by the stronger grain-dominated carbonates, are produced when different lithofacies are juxtaposed at lower displacements, producing a lower permeability range and average value (Fig. 6D, green curve at low displacement), reducing the transmissivity of these low displacement fault zones.

371

372 **Calculating transmissibility multipliers using the outcrop examples**

373 The patterns of fault rock heterogeneity outlined above are now used to upscale the
374 petrophysical properties to model the variation of fault transmissibility with displacement,
375 lithofacies and lithofacies juxtaposition.

376 Since a limited number of deformation mechanisms are active when juxtaposition of similar
377 lithofacies occurs (regardless of lithofacies type), this causes the fault rock heterogeneity to
378 be low and, therefore, to create a reduced range of low permeability values. These factors
379 could cause reduced across-fault flow and generate very low transmissibility multipliers.
380 However, at juxtapositions of different lithofacies, specifically at higher displacements, the
381 large heterogeneity of fault rock types that have been produced causes the range of
382 permeabilities to be high, varying over 7 orders of magnitude (Fig. 6D grain-micrite, green
383 curve). Hence, this reduces or eliminates the possible flow retardation the fault may have,
384 generating transmissibility multipliers of around 1.

385 Figures 7 and 8 show modelled faults of low and high displacement, respectively, using a
386 stratigraphic template based on the Malta LCL-GL sequence of Figure 1. In the first example,
387 with up to 15 m displacement (Fig. 7, Table 1), the transmissibility multipliers are only
388 weakly dependent on lithofacies juxtaposition. As described above, at low displacements
389 <30 m, the fault rock heterogeneity is low, creating a homogeneous low permeability fault
390 core, regardless of juxtaposition type (Fig. 7C). Although some variation occurs, all scenarios
391 at this low displacement create moderately low transmissibility multipliers, which can act to
392 slightly reduce across fault flow. The similar moderately low transmissibility multipliers for

393 all juxtaposition types are calculated despite the large range of area weighted permeability,
394 and hence also transmissibility (Table 1). This is associated with the range of host rock
395 permeabilities; micrite-micrite juxtapositions create fault rocks with significantly lower
396 permeabilities than those created at grain-grain juxtapositions. However, since the micrite-
397 dominated host rock permeability is 2 orders of magnitude lower than the grain-dominated
398 permeabilities, this leads to transmissibility multipliers for micrite-micrite juxtapositions that
399 are very similar than those calculated for grain-grain juxtapositions.

400 At high displacements (Fig. 8), the fault rock heterogeneity is high, caused by an increase in
401 deformation variety and intensity. In the example shown, with up to 90 m displacement
402 (Fig. 8, Table 2), the transmissibility multipliers are heavily dependent on lithofacies
403 juxtaposition. Potential for reduced across-fault flow may occur at micrite-micrite and
404 grain-grain juxtapositions with low transmissibility multipliers created by the low fault rock
405 permeabilities relative to the host rock permeabilities. However, transmissibility multipliers
406 of 1 occur at grain-micrite juxtapositions, eliminating any impairment to flow (red area in
407 centre of Fig. 8F). This is associated with the large variety of fault rock types created on this
408 part of the fault, all with highly variable permeabilities, averaging to produce relatively high
409 fault rock permeability values and hence high transmissibility multipliers (Table 2, Fig. 8).

410

411 **Discussion**

412 It is well known that juxtaposing different siliciclastic lithologies, e.g. shale against
413 sandstone, can lead to mixing of the two lithologies to create a shaley gouge (Yielding *et al.*
414 1997). However, the implications on fault rock development of carbonate lithofacies

juxtaposition, where shaley beds are rare or absent, is much less documented. We have shown that the use of measured permeability variations from outcrop samples has allowed us to make preliminary calculations of potential fault rock permeability, and therefore transmissibility multipliers, in a range of different scenarios (host lithofacies, displacements and juxtaposition types). It is these three controlling factors that we have used to predict the transmissibility multipliers in a cellular grid based on the Malta stratigraphic sequence.

Using these specific results, it is possible to start to extend the calculations to a range of carbonate sequences with lithofacies like those on Malta, but varying their unit thicknesses. As shown in Figure 9, examples include: a micrite-dominated sequence, a grain-dominated sequence, a sequence containing thin interbeds, or alternating units with similar thicknesses of micrite- and grain-dominated carbonates. In all cases, micrite-dominated carbonates have high porosity and low permeability, grain-dominated carbonates have high porosity and high permeability. A sequence with consistent similar lithofacies (whether this is low permeability micrite-dominated carbonates or high permeability grain-dominated carbonates) is likely to create a baffle with low transmissibility multipliers, as this scenario will limit the variety of fault rock types produced and hence will also limit the range of permeability to low values (Fig. 9A and B). A sequence with minor proportions of different lithofacies may create transmissive areas where different lithofacies juxtapositions occur (Fig. 9C and D). However, the overall fault transmissibility for these scenarios may be dependent on bed thickness, as a sequence with thin interbeds of different lithofacies may not have significant control on the variety of different fault rock types produced, and therefore on the overall permeability variation. Such scenarios require further research to

verify the significance of interbeds on the transmissibility multipliers at their areas of overlap. Faults cutting a sequence with variable lithofacies and similar bed thicknesses are not likely to impact flow, because of the potential increase in the number of fault rock types at the point of different lithofacies juxtapositions, all with variable permeabilities, which are likely to create a high average permeability and hence high transmissibility multipliers at these areas of overlap (Fig. 9E).

It is important to note that the predictions of fault rock permeability and transmissibility multipliers outlined above have not been tested. These predictions are based solely on how two end member lithofacies deform under different scenarios, which may or may not translate to other carbonate scenarios with similar lithofacies. Through continued research we will aim to gather more information to support or reject these predictions.

Further to this, the Maltese analogue in this study restricts us to only two end-members, both with high porosities (*c.*30%) but variable permeabilities. It is important to note that the calculations of fault transmissibility can only strictly be applied to the faulted carbonate sequence on Malta. The same methodology could be applied in other carbonate lithofacies (such as those with low porosities), using previously documented permeabilities (e.g. Agosta 2008). However, there are very few published examples, so the uncertainty is high. Continued research is required to advance and test these calculations. By increasing our knowledge of how different lithofacies deform, the fault rocks that are produced and their permeability, we are hopeful that it will be possible to predict fault transmissibility for different carbonate stratigraphy as a function of fault throws.

458 Not only will the fault rock thickness and permeability have an impact on the transmissibility
459 of faults, but the entire fault zone architecture will dictate the distribution and hence
460 location of fault rock. A zone of intense deformation bound by and incorporating several
461 slip surfaces occurs within the Maltese fault zones when juxtaposition of different
462 lithofacies of varied strength occurs (Fig. 3). This distributed strain will, therefore, have
463 significant control over the location of fault rock formation. The transmissibility multiplier
464 calculation retains the assumption that there is a continuous fault core along the length of
465 the fault. However, as shown in previous research of these faults, this does not occur until
466 higher displacement when there is juxtaposition of different lithofacies (Michie *et al*. 2014).
467 Therefore, although relatively low transmissibility multipliers are calculated here for a fault
468 zone of low displacement, this may not always be the case, depending on the fault zone
469 architecture.

470

471 **Summary**

472 We have attempted to calculate and predict the transmissibility of carbonate-hosted
473 extensional fault zones by using field and laboratory data of carbonate fault rocks in two
474 different lithofacies. Knowledge of how lithofacies deform, the microstructures produced
475 when faulted, their permeabilities and the patterns to the fault rocks produced, aids this
476 prediction. Fault rock types are observed to vary with host lithofacies, displacement and
477 juxtaposition (Fig. 10). Strength and textural differences between the two lithofacies cause
478 the greatest microstructural variation, by controlling the principal deformation mechanisms
479 between these lithofacies. The degree of deformation adds complexities to the fault rocks

480 produced, creating a greater variety of more complex fault rocks at higher displacements.
481 How the two lithofacies are juxtaposed also alters the fault rock types; juxtaposition of
482 similar lithofacies restricts the deformation style, creating fewer fault rock types. Each of
483 these factors also controls the fault rock permeability and the resultant transmissibility
484 multipliers (Fig. 10).

485 A smaller variety of fault rock types with more homogeneous microstructures occurs at
486 displacements <30 m, and all have low permeabilities reducing the transmissibility
487 multipliers, regardless of juxtaposition type. Juxtaposition of different lithofacies at
488 displacement >30 m creates a wide variety of fault rocks, all with variable poroperm values,
489 which average out to create negligible impact on fluid flow, with transmissibility multipliers
490 of around 1. However, juxtaposition of similar lithofacies at these higher displacements
491 reduces the variability of both microstructures and permeability, lowering the
492 transmissibility multipliers (Fig. 10).

493 Although this study allows us to predict fault transmissibility multipliers in two carbonate
494 lithofacies on Malta with high porosities, the transmissibility of faults in carbonate
495 sequences and/or structural settings in general may well show different behaviour. Hence,
496 more work is being undertaken, using outcrop and subsurface data, in order to predict the
497 transmissibility of faults in a wider range of settings. We aim to gather more data from
498 different lithofacies, depth of burial, tectonic regimes etc. to advance this research.

499

Acknowledgments

We thank T. Haines for much help with sample collection, preparation and measurements, and C. Taylor for technical assistance in the lab. We also thank P. Bretan and A. Foster for help with software implementation, as well as D. Sanderson and an anonymous reviewer for their constructive comments that improved the quality of this manuscript.

References

Agosta, F., & Kirschner, D. L. 2003. Fluid conduits in carbonate-hosted seismogenic normal faults of central Italy. *Journal of Geophysical Research*, **108**(B4), 2221.

Agosta, F. 2008. Fluid flow properties of basin-bounding normal faults in platform carbonates, Fucino Basin, central Italy. *Geological Society, London, Special Publications*, **299**, 277–291.

Antonellini, M., & Aydin, A. 1994. Effect of faulting on fluid flow in porous sandstones: petrophysical properties. *AAPG Bulletin*, **78**(3), 355–377.

Antonellini, M., & Mollema, P. N. 2000. A natural analog for a fractured and faulted reservoir in dolomite: Triassic Sella Group, northern Italy. *AAPG Bulletin*, **84**, 314–344. doi:10.1306/C9EBCDDD-1735-11D7-8645000102C1865D

Aydin, A. and Eyal, Y. 2002. Anatomy of a normal fault with shale smear: Implications for fault seal. *AAPG Bulletin*, **86**, 8, 1367-1381.

Bastesen, E., & Braathen, A. 2010. Extensional faults in fine grained carbonates - analysis of fault core lithology and thickness-displacement relationships. *Journal of Structural Geology*, **32**(11), 1609–1628. doi:10.1016/j.jsg.2010.09.008

Bastesen, E., Braathen, A., Nøttveit, H., Gabrielsen, R. H., & Skar, T. 2009. Extensional fault cores in micritic carbonate – Case studies from the Gulf of Corinth, Greece. *Journal of Structural Geology*, **31**(4), 403–420.

Billi, A., Valle, A., Brilli, M., Faccenna, C., & Funiciello, R. 2007. Fracture-controlled fluid circulation and dissolutional weathering in sinkhole-prone carbonate rocks from central Italy. *Journal of Structural Geology*, **29**, 385–395. doi:10.1016/j.jsg.2006.09.008

Bonson, C. G., Childs, C., Walsh, J. J., Schopfer, M. P. J., & Carboni, V. 2007. Geometric and kinematic controls on the internal structure of a large normal fault in massive limestones: The Maghlaq Fault, Malta. *Journal of Structural Geology*, **29**(2), 336–354.

531 Caine, J. S., Evans, J. P., & Forster, C. B. 1996. Fault zone architecture and permeability
532 structure. *Geology*, **24**(11), 1025–1028.

533 Chester, F. M., & Logan, J. M. 1986. Implications for mechanical properties of brittle faults
534 from observations of the Punchbowl Fault Zone, California. *Pure and Applied Geophysics*,
535 **124**(1-2), 79–106.

536 Crawford, B. R., Myers, R. ., Woronow, A., Faulkner, D. R., & Rutter, E. H. 2002. Porosity-
537 permeability relationships in clay-bearing fault gouge: Presented at the Society of Petroleum
538 Engineers/International Society of Rock Mechanics, Rock Mechanics Conference, Irving,
539 Texas, October 20-23,. *SPE/ISRM 78214*, 13p.

540 Dart, C. J., Bosence, D. W. J., & McClay, K. R. 1993. Stratigraphy and structure of the Maltese
541 graben system. *Journal of the Geological Society*, **150**(6), 1153–1166.

542 Dunham, R.J. 1962. Classification of carbonate rocks according to depositional texture. *In:*
543 Ham, W.E. (ed.) *Classification of Carbonate Rocks*. American Association of Petroleum
544 Geologists Memoir, 1, 108-121

545 Ehrenberg, S.N., and Nadeau, P.H. 2003. Sandstone vs. carbonate petroleum reservoirs: A
546 global perspective on porosity-depth and porosity-permeability relationships. *AAPG Bulletin*,
547 **89**, 435-445.

548 Evans, J. P., Forster, C. B., & Goddard, J. V. 1997. Permeability of fault-related rocks, and
549 implications for hydraulic structure of fault zones. *Journal of Structural Geology*, **19**(11),
550 1393–1404.

551 Færseth, R. B., Johnsen, E., & Sperrevik, S. 2007. Methodology for risking fault seal capacity:
552 Implications of fault zone architecture. *AAPG Bulletin*, **91**(9), 1231–1246.

553 Fisher, Q. J., & Knipe, R. J. 1998. Fault sealing processes in siliciclastic sediments. *In: Jones,*
554 *G., Fisher, Q. J. & Knipe, R. J. (eds) Faulting, Fault Sealing and Fluid Flow in Hydrocarbon*
555 *Reservoirs. Geological Society, London, Special Publications*, **147**, 117–134.

556 Fisher, Q., & Knipe, R. 2001. The permeability of faults within siliciclastic petroleum
557 reservoirs of the North Sea and Norwegian Continental Shelf. *Marine and Petroleum*
558 *Geology*, **18**(2001), 1063–1081.

559 Flodin, E., Gerdes, M., Aydin, A., & Wiggins, W. 2005. Petrophysical properties and sealing
560 capacity of fault rock, Aztec Sandstone, Nevada. *In: R. Sorkhabi and Y. Tsuji, (eds). Faults,*
561 *Fluid Flow, and Petroleum Traps: AAPG Memoir*, **85**, 197–218.

562 Foxford, K. a., Walsh, J. J., Watterson, J., Garden, I. R., Guscott, S. C., & Burley, S. D. 1998.
563 Structure and content of the Moab Fault Zone, Utah, USA, and its implications for fault seal
564 prediction. *Geological Society, London, Special Publications*, **147**, 87–103.
565 doi:10.1144/GSL.SP.1998.147.01.06

566 Fulljames, J., Zijerveld, L., & Franssen, R. 1997. Fault seal processes: systematic analysis of
567 fault seals over geological and production time scales. *In: Møller-Pedersen, P. Koestler, A. G.,*

568 *(eds) Hydrocarbon Seals: Importance for Exploration and Production. Special Publication of*
569 *the Norwegian Petroleum Society*, **7**, 51–59.

570 Giurgea, V., Rettenmaier, D., Pizzino, L., Unkel, I., Hötzl, H., Förster, A., & Quattrocchi, F.
571 2004. Preliminary hydrogeological interpretation of the Aigion area from the AIG10
572 borehole data. *Comptes Rendus Geoscience*, **336**(4-5), 467–475.
573 doi:10.1016/j.crte.2003.12.012

574 Groshong, R. 1988. Low-temperature deformation mechanisms and their interpretation.
575 *Geological Society of America Bulletin*, **100**, 1329–1360.

576 House, M. R, Dunham, K. C, Wigglesworth, J. C. 1961. Geology of the Maltese Islands. *In:*
577 *Malta, Background for Development. H. Bowen-Jones, J. C. Dewdney, W. B. Fisher (eds) Univ.*
578 *Durham*, 24–33.

579 Hull, J. 1988. Thickness-displacement relationships for deformation zones. *Journal of*
580 *Structural Geology*, **10**(4), 431–435.

581 Klinkenberg, L. J. 1941. The permeability of porous media to liquids and gases. *Drilling and*
582 *Production Practice*, 200–213.

583 Knipe, R. J. 1992. Faulting processes and fault seal. *In: Structural and Tectonic Modelling and*
584 *Its Application to Petroleum Geology, R. M Larsen, H. Brekke, B. T. Larsen, E. Talleras (Eds.)*
585 *Amsterdam, Elsevier*, **1**, 325–342.

586 Knipe, R. J. 1997. Juxtaposition and seal diagrams to help analyze fault seals in hydrocarbon
587 reservoirs. *AAPG Bulletin*, **81**(2), 187–195. doi:10.1306/522B42DF-1727-11D7-
588 8645000102C1865D

589 Knott, S. D., Beach, A., Brockbank, P. J., Lawson Brown, J., McCallum, J. E., & Welbon, A. I.
590 1996. Spatial and mechanical controls on normal fault populations. *Journal of Structural*
591 *Geology*, **18**, 359–372. doi:10.1016/S0191-8141(96)80056-3

592 Kranz, R. 1983. Microcracks in rocks: a review. *Tectonophysics*, **100**, 449–480.

593 Lucia, F., Kerans, C., & Jennings, J. 2003. Carbonate Reservoir Characterization. *Journal of*
594 *Petroleum Technology*, **55**(06), 70–72. doi:10.2118/82071-MS

595 Manzocchi, T., Walsh, J. J., Nell, P., & Yielding, G. 1999. Fault transmissibility multipliers for
596 flow simulation models. *Petroleum Geoscience*, **5**, 53–63. doi:10.1144/petgeo.5.1.53

597 Micarelli, L., Benedicto, A., & Wibberley, C. A. J. 2006. Structural evolution and permeability
598 of normal fault zones in highly porous carbonate rocks. *Journal of Structural Geology*, **28**(7),
599 1214–1227.

600 Michie, E. A. H. 2015. Influence of host lithofacies on fault rock variation in carbonate fault
601 zones: A case study from the Island of Malta. *Journal of Structural Geology*, **76**, 61–79.
602 doi:10.1016/j.jsg.2015.04.005

603 Michie, E. A. H., Haines, T. J., Healy, D., Neilson, J. E., Timms, N. E., & Wibberley, C. A. J.
604 2014. Influence of carbonate facies on fault zone architecture. *Journal of Structural Geology*,
605 **65**, 82–99. doi:10.1016/j.jsg.2014.04.007

606 Pedley, H. M., House, M. R., & Waugh, B. 1976. The geology of Malta and Gozo. *Proceedings*
607 *of the Geologists' Association*, **87**(3), 325–341.

608 Shipton, Z. K., & Cowie, P. A. 2003. A conceptual model for the origin of fault damage zone
609 structures in high-porosity sandstone. *Journal of Structural Geology*, **25**(3), 333–344.

610 Tondi, E. 2007. Nucleation, development and petrophysical properties of faults in carbonate
611 grainstones: Evidence from the San Vito Lo Capo peninsula (Sicily, Italy). *Journal of Structural*
612 *Geology*, **29**(4), 614–628.

613 Tucker, M. E., & Wright, V. P. 2009. *Carbonate Sedimentology*. John Wiley & Sons.

614 Van der Land, C., Wood, R., Wu, K., van Dijke, M. I. J., Jiang, Z., Corbett, P. W. M., & Couples,
615 G. 2013. Modelling the permeability evolution of carbonate rocks. *Marine and Petroleum*
616 *Geology*, **48**, 1–7. doi:10.1016/j.marpetgeo.2013.07.006

617 Walsh. J. J., Watterson, J., Heath, A. E., Childs, C. 1998. Representation and scaling of faults
618 in fluid flow models. *Petroleum Geoscience*, **4**(3), 241-251.

619 Yielding, G. 2015. Trapping of buoyant fluids in fault-bound structures. *Geological Society,*
620 *London, Special Publications*, **421**(SP421-3).

621 Yielding, G., Freeman, B., & Needham, D. 1997. Quantitative fault seal prediction. *AAPG*
622 *Bulletin*, **6**(6), 897–917.

623

624 **Figure Captions**

625 **Fig. 1.** Map of Malta showing the main faults and their trends. Two main localities on Malta
626 used for examination of several faults are highlighted in boxes: Ras ir Raheb and Madliena
627 Tower. IMF: Il Maqhlaq fault. VLF: Victoria Lines Fault. A simplified stratigraphic log
628 through the Oligo-Miocene sequence is also shown. Classification from Dunham (1962).

629

Fig. 2. Optical photomicrographs and SEM images of the two host lithofacies, micrite-dominated (A) and grain-dominated (B) carbonates, showing their textural differences, as well as a poroperm plot of these host rocks (C). Micrite-dominated carbonates are fine-grained, with high porosity but low permeability. Grain-dominated carbonates are coarser grained, with high porosity and high permeability.

Fig. 3. A: Field photograph of a 7 m displacement fault zone at Ras ir Raheb showing an example of fault architecture. Red lines indicate slip surfaces. (I) Lower hemisphere stereonet showing poles to both faults (red) and fractures (grey) striking ENE-WNE, dipping southward. B: 3D block model of the 7m fault in A, showing the along strike and down dip variability to the fault zone. C: Schematic diagram of the faults offsetting micrite-dominated carbonates next to grain-dominated carbonates: a fault-bounded, intensely deformed damage zone (IDDZ) named the fracture splay zone (FSZ), surrounded by a weakly deformed damaged zone (WDDZ). Fault cores occur on one or more of the slip surfaces.

Fig. 4. Schematic diagram showing the averaging techniques used to upscale measured permeability and thickness variations to model a fault in a cellular grid, in order to predict flow across a fault. Averaging techniques for permeability shown in black (bottom), and thickness shown in red (top). Geometric averages are calculated for permeability variation between fault rock samples, which are then arithmetically averaged to upscale the fault-rock permeability component to a reservoir connection (black arrows). Arithmetic averages

651 are calculated for thickness variation between mapped fault rock thicknesses, which are
652 then harmonically averaged to upscale the thickness component to a reservoir connection
653 (red arrows).

654

655 **Fig. 5.** Optical photomicrographs, SEM image and hand specimen photographs showing the
656 microstructures observed in the damage zone (damaged rock, A & B) and fault core (fault
657 rock, C & D) of the two lithofacies; micrite-dominated (A & C) and grain-dominated (B & D)
658 carbonates. A1: fractured (f) rock with intact fossil clasts. A2: intact rock showing no
659 deformation or diagenetic microstructures. B1: Clast confined fractures, creating
660 microbreccia (b). Hz: Hertzian impingement microcracks. B2: Cemented rock. Mi: Micrite.
661 Sp: Sparite. C1: Incohesive mosaic breccia. C2: Indurated chaotic breccia. C3: Recrystallised
662 fault rock. w: Wavy crystal boundaries. D1: Cataclasite. Rd: Rounded cataclased clasts. D2:
663 Cemented fault rock. D3: Composite chaotic breccia. bc: Breccia clasts.

664

665 **Fig. 6.** Poroperm plot of all sampled fault rocks (A). Frequency curves of permeability
666 shown with increasing fault displacement (B), subdivided into lithofacies (C) and lithofacies
667 juxtaposition (D). Permeability of the protolith shown on the Y axis (at 0 m displacement).
668 B shows how the individual permeability data-points were used to construct frequency
669 histograms (horizontal bars); the frequency curve is then drawn through the centre of each
670 bar. For clarity, data-points and histograms are not shown in C and D.

671

672 **Fig. 7.** Fault rock permeability and transmissibility multipliers calculated in TrapTester-T7
673 for a fault zone of up to 15 m displacement, cutting through two carbonate lithofacies, using
674 patterns to fault rock permeability variation observed from Malta. The 20 layer model is
675 195 m thick, with a 916 m long fault (5 cells along the fault length). Geometry of the fault is
676 shown in a 3D view at the bottom, with cells infilled with protolith permeability values.
677 Diagrams A-D are shown in fault-strike view. The synthetic log with added noise used to
678 populate the cells is shown to the left, porosity (green) and permeability (purple); similar
679 porosity occurs throughout the sequence, varying from 25 to 35%, with the permeability
680 varying at the lithofacies boundary from *c.* 200 mD in the lower half to *c.* 2 mD in the upper
681 half of the section.

682

683 **Fig. 8.** Fault rock permeability and transmissibility multipliers calculated in TrapTester-T7
684 for a 60 m displacement fault cutting through two carbonate lithofacies, using patterns to
685 fault rock permeability variation observed from Malta. The 20 layer model is 195 m thick,
686 and the fault is 1833 m long (10 cells along the fault length), after Manzocchi *et al.* (1999).
687 Geometry of the fault is shown in a 3D view, with cells infilled with protolith permeability
688 values (colour key on B and C). The fault has an out-of-plane footwall splay. Diagrams A-F
689 are shown in strike view. Synthetic log with added noise used to populate the cells is shown
690 to the right; porosity (green) and permeability (purple); similar porosity occurs throughout
691 the sequence, varying from 25 to 35%, with the permeability varying at the lithofacies
692 boundary from *c.* 200 mD in the lower half to *c.* 2 mD in the upper half of the section.

693

Fig. 9. Predictions of the transmissibility multipliers in different stratigraphic scenarios using the same fault as shown in Figure 8, varying the proportion of micrite-dominated (low permeability <10 mD) and grain-dominated (high permeability >100 mD) carbonates. A and B: similar lithofacies continuously through the sequence. D and C: thin interbeds. E: varying lithofacies with similar unit thicknesses. Synthetic logs used to populate the cells are shown: porosity (green) and permeability (purple); similar porosity occurs throughout the sequence, but with the permeability varying at the lithofacies proportions.

Fig. 10. Schematic showing how the permeability, porosity and transmissibility multipliers (trans mult) varies with lithofacies and juxtaposition types at two different displacements in the Malta carbonate sequence.

Table Captions

Table 1. Transmissibility and transmissibility multipliers manually calculated for an 11.7 m displacement fault zone at different lithofacies juxtapositions. Numbers are based on a cell-dimension of 150 m.

Table 2. Transmissibility and transmissibility multipliers manually calculated for a 90 m displacement fault zone at different lithofacies juxtapositions. Numbers are based on a cell-dimension of 150 m.

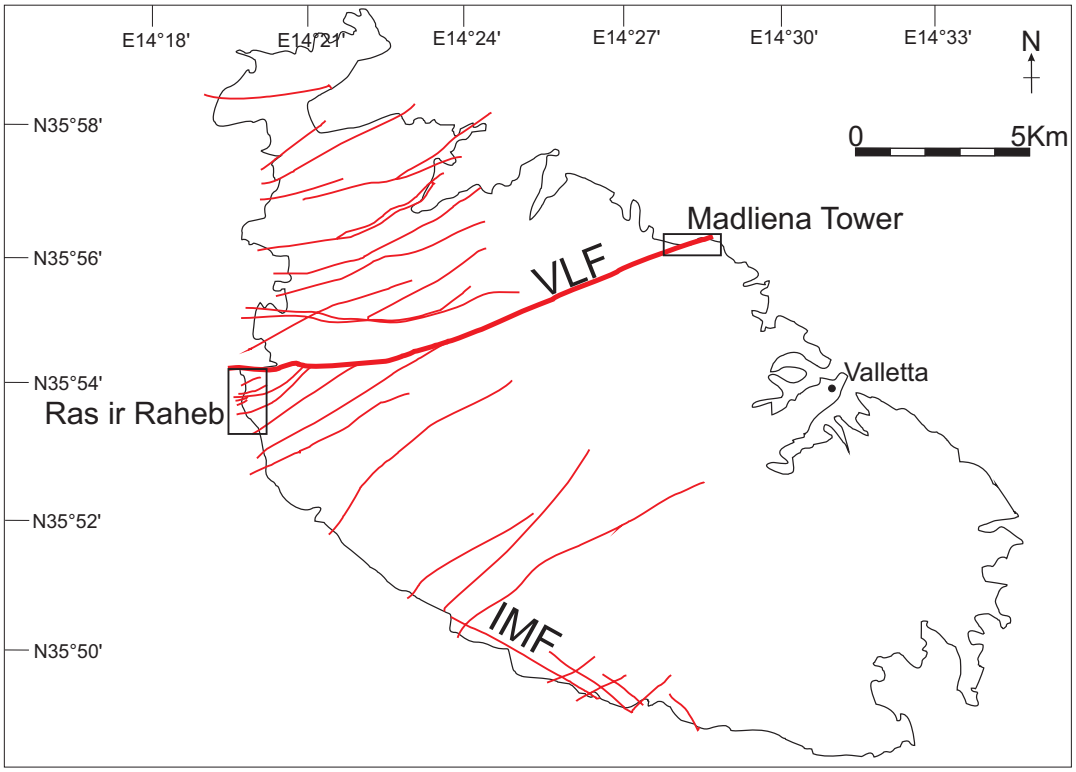
E14°18'
E14°21'
E14°24'
E14°27'
E14°30'
E14°33'
N
N35°58'
N35°56'
N35°54'
N35°52'
N35°50'
0
5Km
Madliena Tower
VLF
Valletta
Ras ir Raheb
IMF

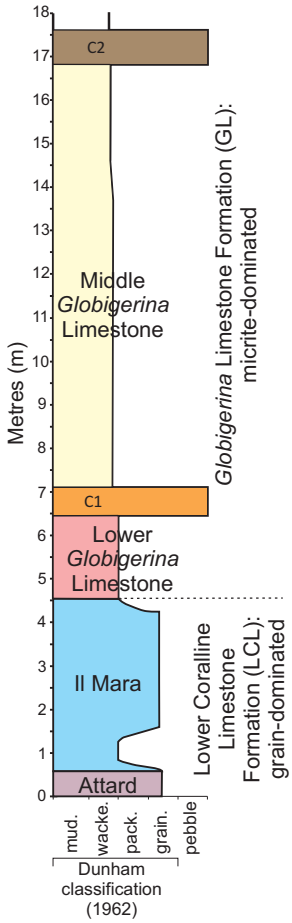
Metres (m)
C2
Middle
Globigerina
Limestone
Globigerina Limestone Formation (GL):
micrite-dominated
C1
Lower
Globigerina
Limestone
Il Mara
Attard
Lower Coralline
Limestone
Formation (LCL):
grain-dominated
mud.
wacke.
pack.
grain.
pebble
Dunham
classification
(1962)

Micrite-dominated

A

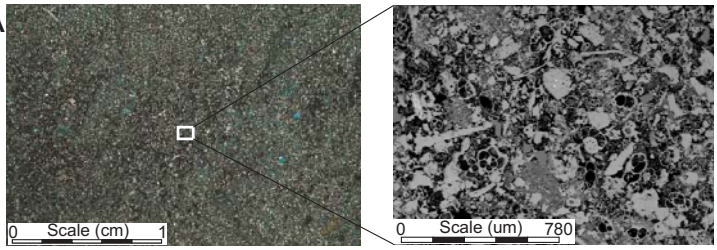

Fine-grained, micrite-supported. Intact fossil clasts. High (*c.*33%) porosity, low strength (40 MPa), low permeability (*c.*2mD).

Grain-dominated

B

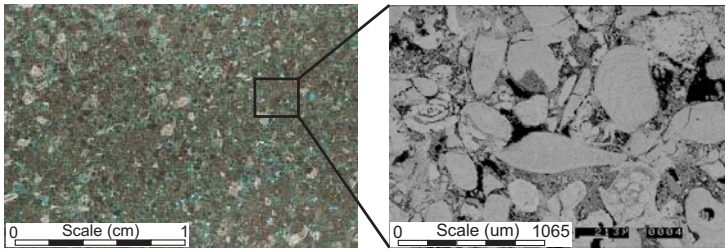

Coarse-grained, grain-supported with some micrite infilling pores. Intact fossil clasts. High (*c.*26%) porosity, high strength (80 MPa), high permeability (*c.*200 mD)

C

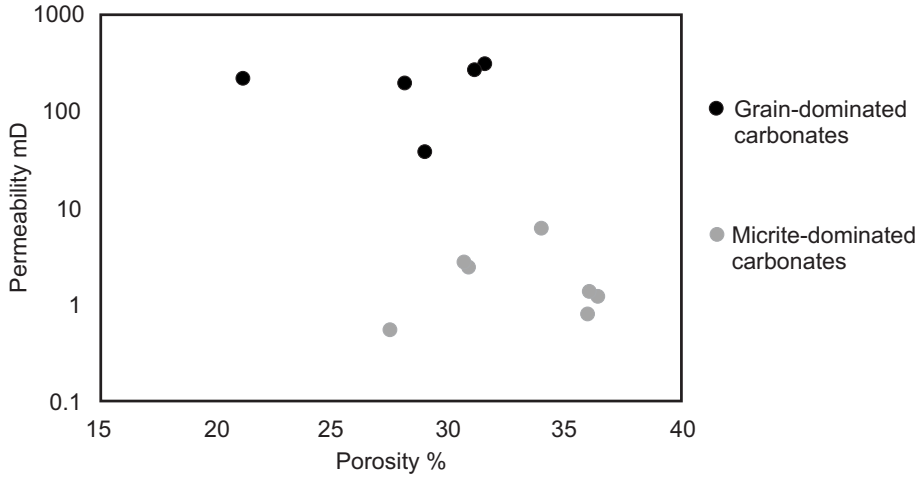

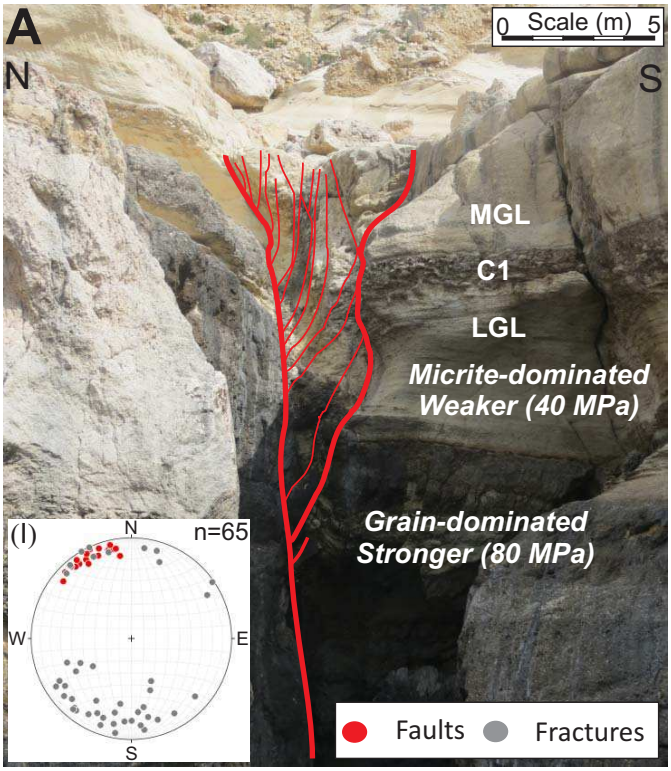
A
N
S
0 Scale (m) 5
MGL
C1
LGL
Micrite-dominated
Weaker (40 MPa)
Grain-dominated
Stronger (80 MPa)
(I)
N
n=65
W
E
S
Faults
Fractures

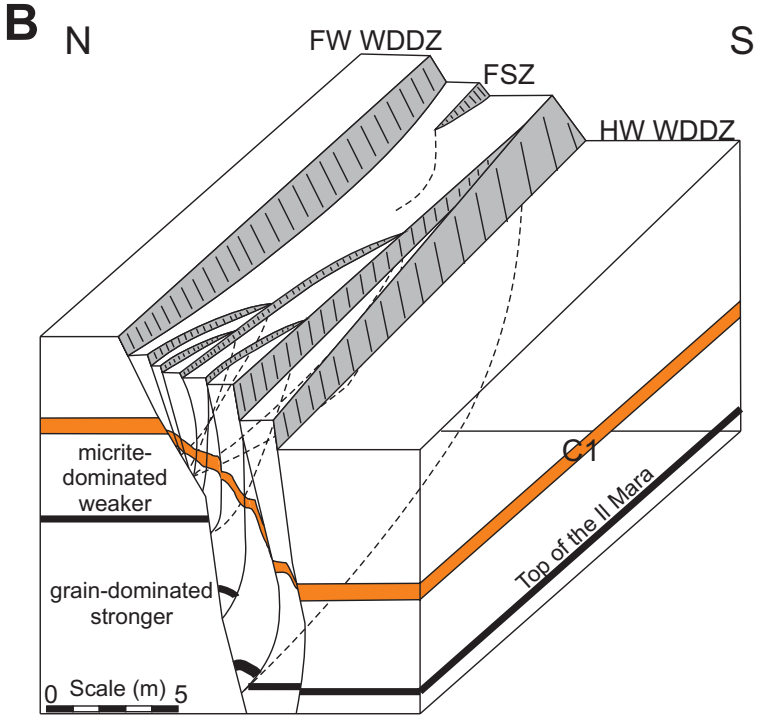
B
N
S
FW WDDZ
FSZ
HW WDDZ
micrite-
dominated
weaker
grain-dominated
stronger
C1
Top of the II Mara
0 Scale (m) 5

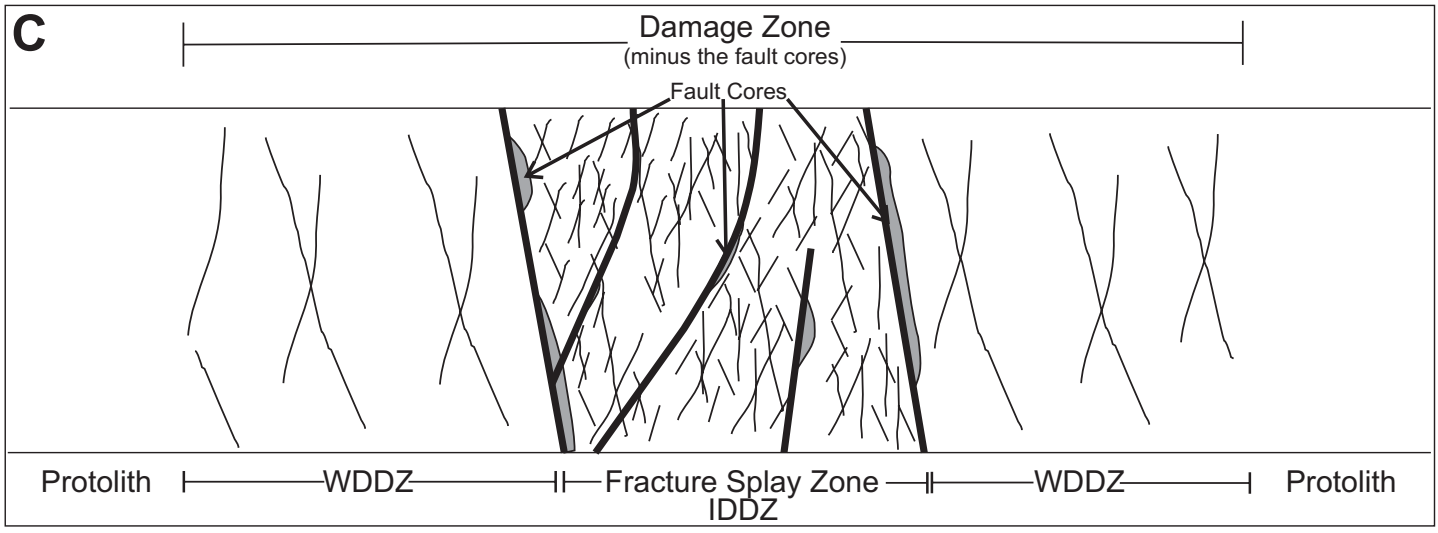
C
Damage Zone
(minus the fault cores)
Fault Cores
Protolith
WDDZ
Fracture Splay Zone
IDDZ
WDDZ
Protolith

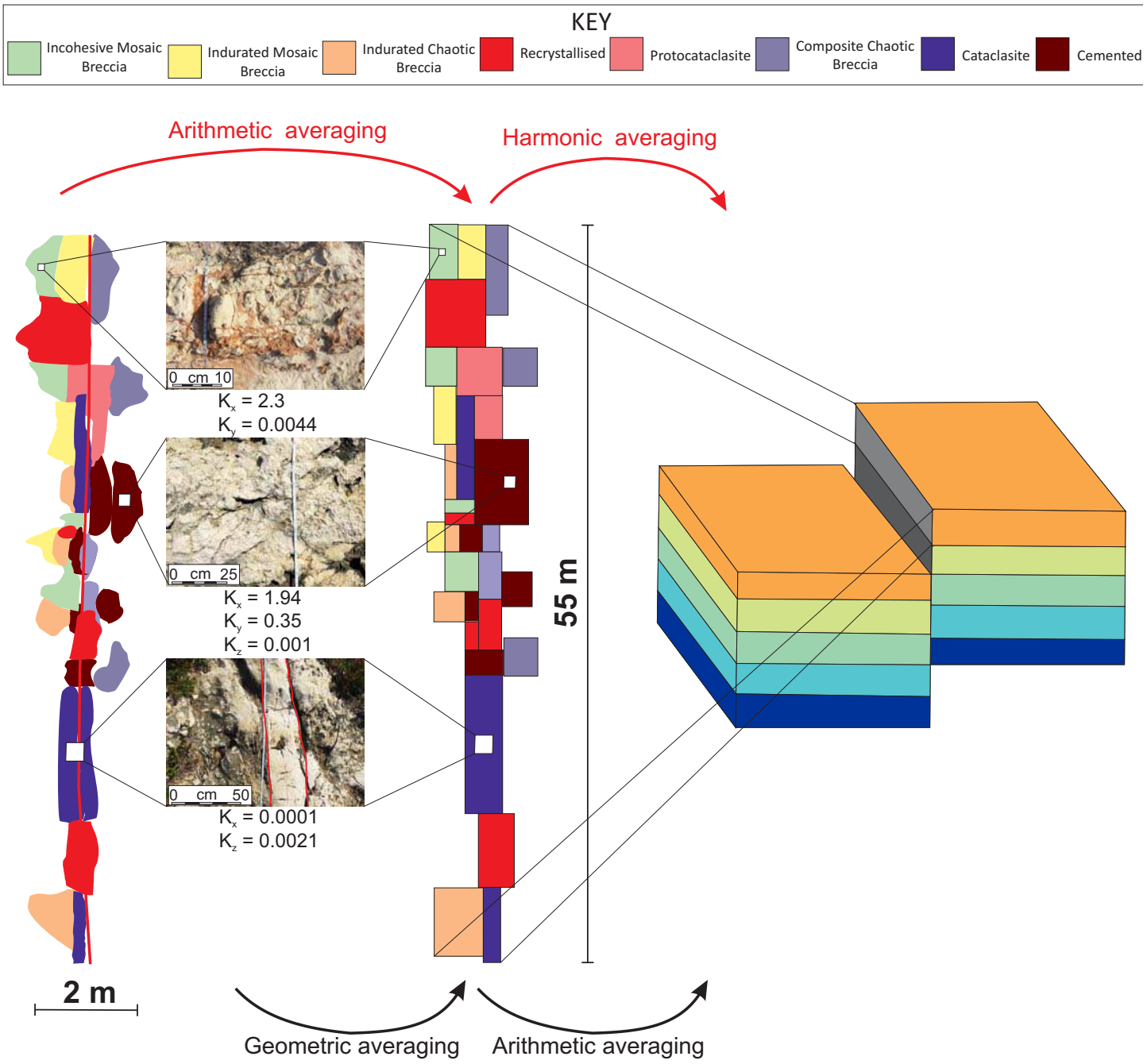
KEY
Incohesive Mosaic Breccia
Indurated Mosaic Breccia
Indurated Chaotic Breccia
Recrystallised
Protocataclasite
Composite Chaotic Breccia
Cataclasite
Cemented
Arithmetic averaging
Harmonic averaging
0 cm 10
K_x = 2.3
K_y = 0.0044
0 cm 25
K_x = 1.94
K_y = 0.35
K_z = 0.001
0 cm 50
K_x = 0.0001
K_z = 0.0021
55 m
2 m
Geometric averaging
Arithmetic averaging

Micrite-dominated

Grain-dominated

Damaged Rock

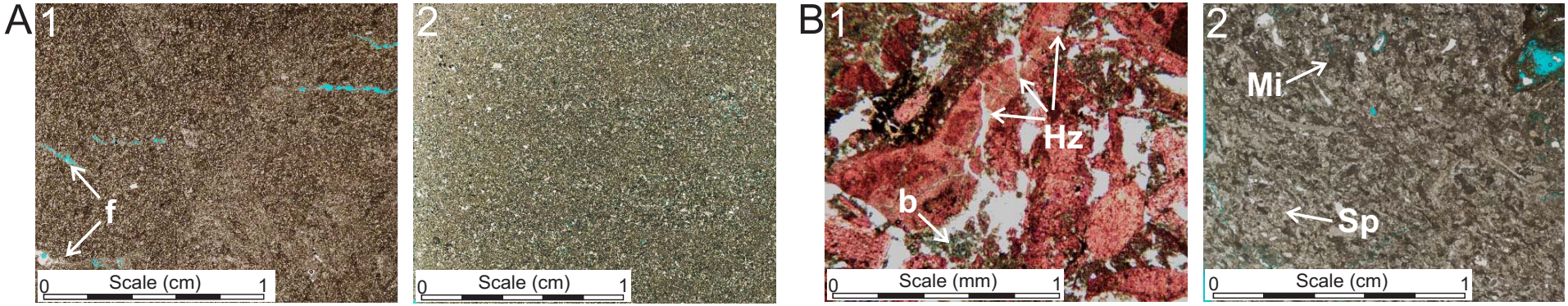

Fault Rock

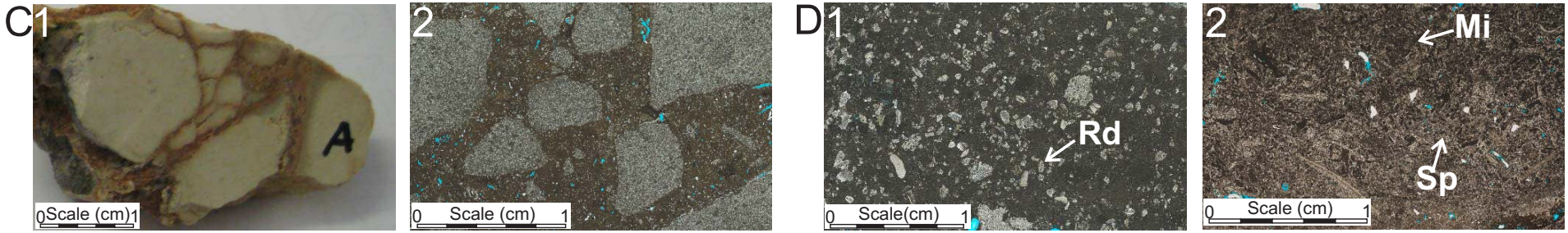

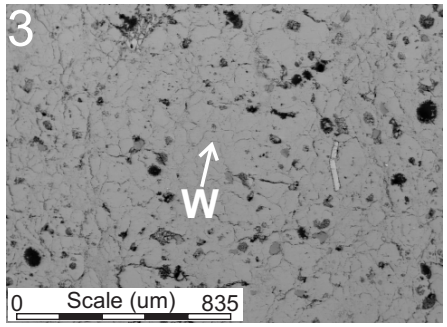

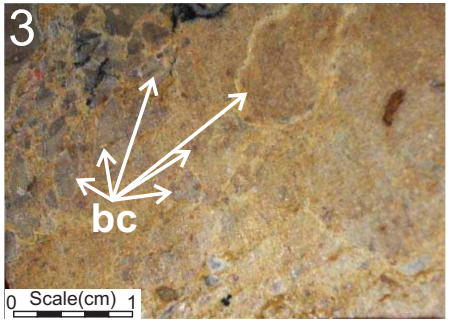

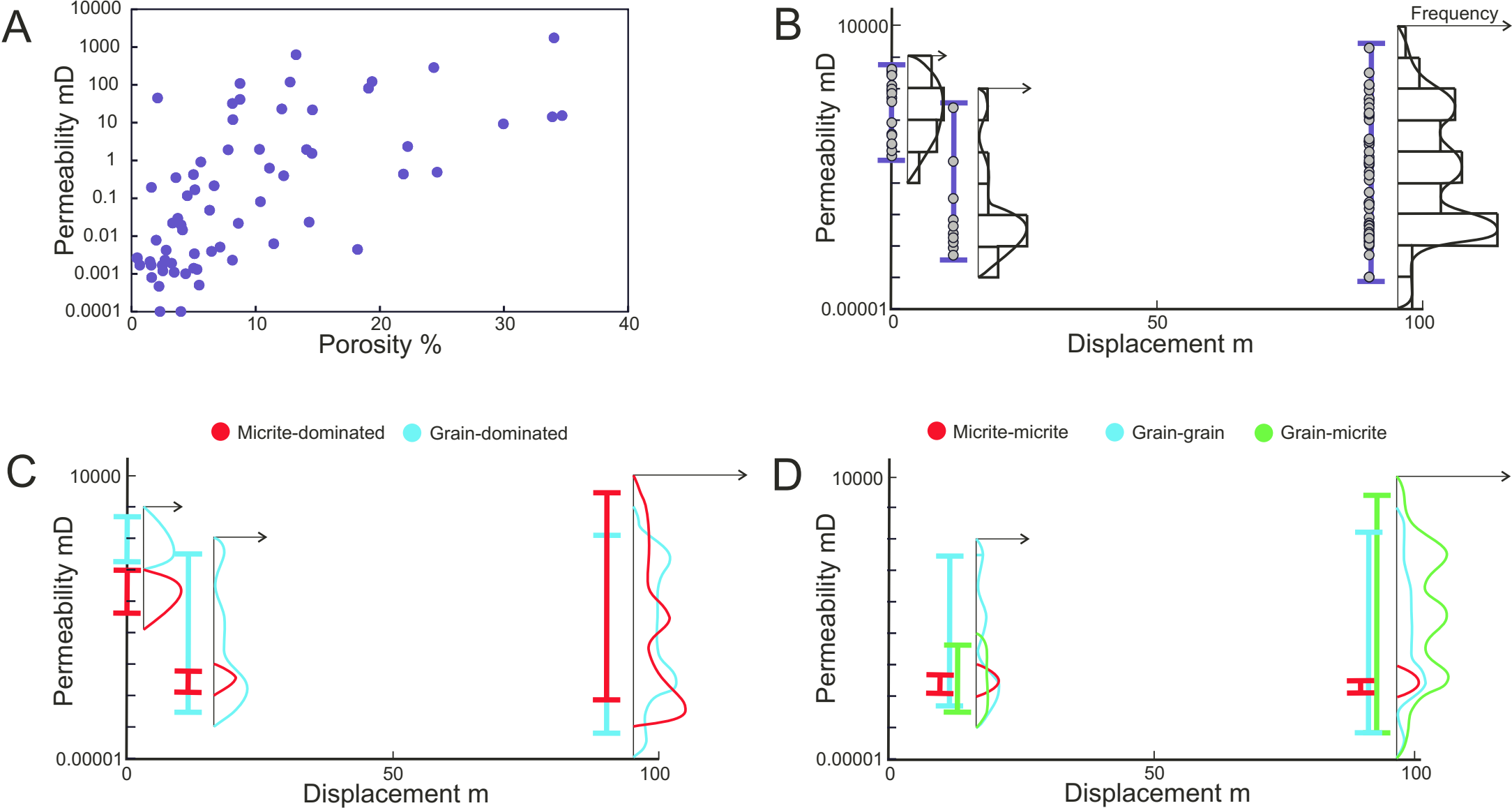
A
Permeability mD
10000
1000
100
10
1
0.1
0.01
0.001
0.0001
0
10
20
30
40
Porosity %
B
Permeability mD
10000
0.00001
0
50
100
Displacement m
Frequency
C
Micrite-dominated
Grain-dominated
Permeability mD
10000
0.00001
0
50
100
Displacement m
D
Micrite-micrite
Grain-grain
Grain-micrite
Permeability mD
10000
0.00001
0
50
100
Displacement m

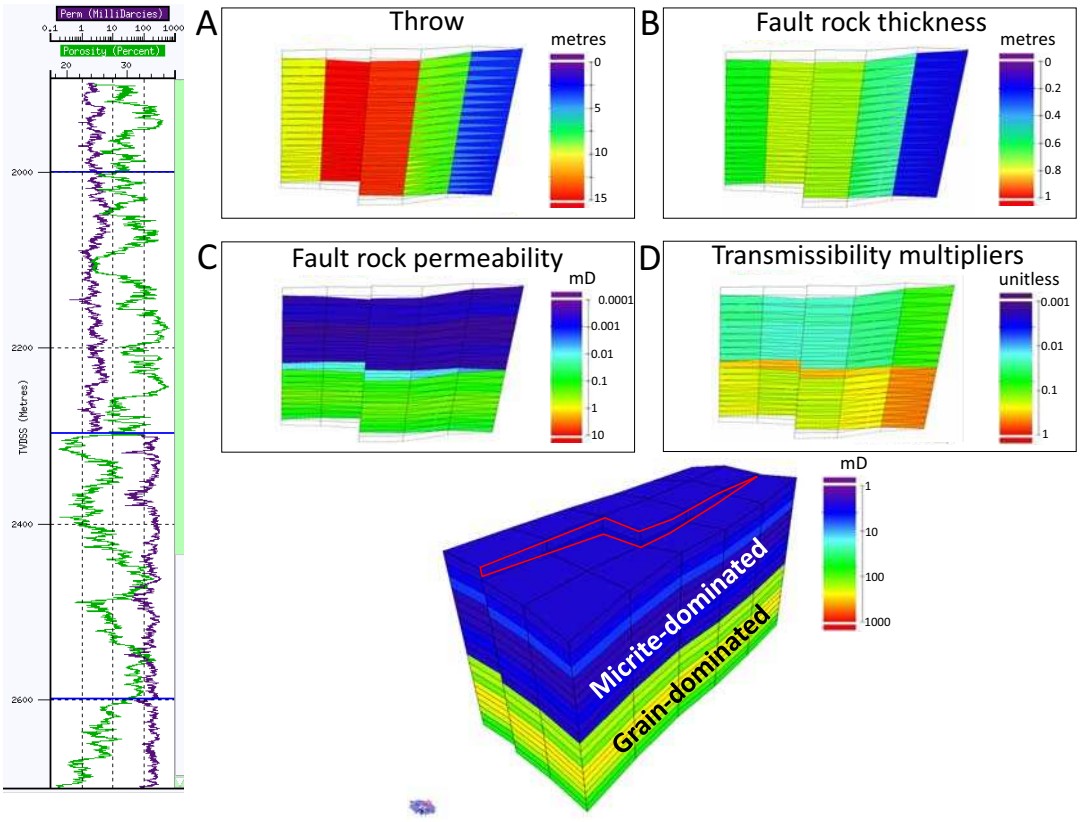
Perm (MilliDarcies)
0.1
1
10
100
1000
Porosity (Percent)
20
30
2000
2200
2400
2600
TVDSS (Metres)
A
Throw
metres
0
5
10
15
B
Fault rock thickness
metres
0
0.2
0.4
0.6
0.8
1
C
Fault rock permeability
mD
0.0001
0.001
0.01
0.1
1
10
D
Transmissibility multipliers
unitless
0.001
0.01
0.1
1
mD
1
10
100
1000
Micrite-dominated
Grain-dominated

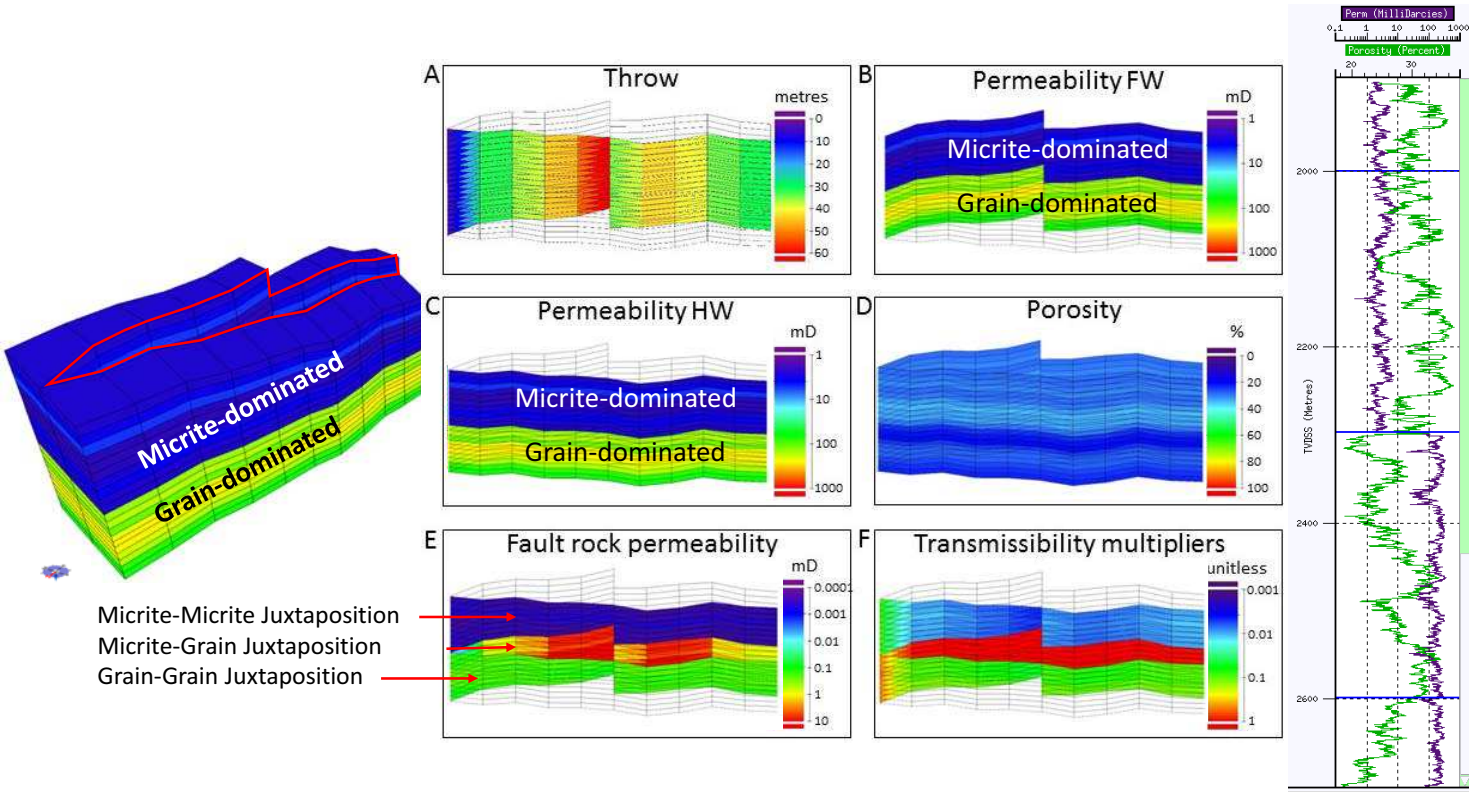

Micrite-Micrite Juxtaposition
Micrite-Grain Juxtaposition
Grain-Grain Juxtaposition

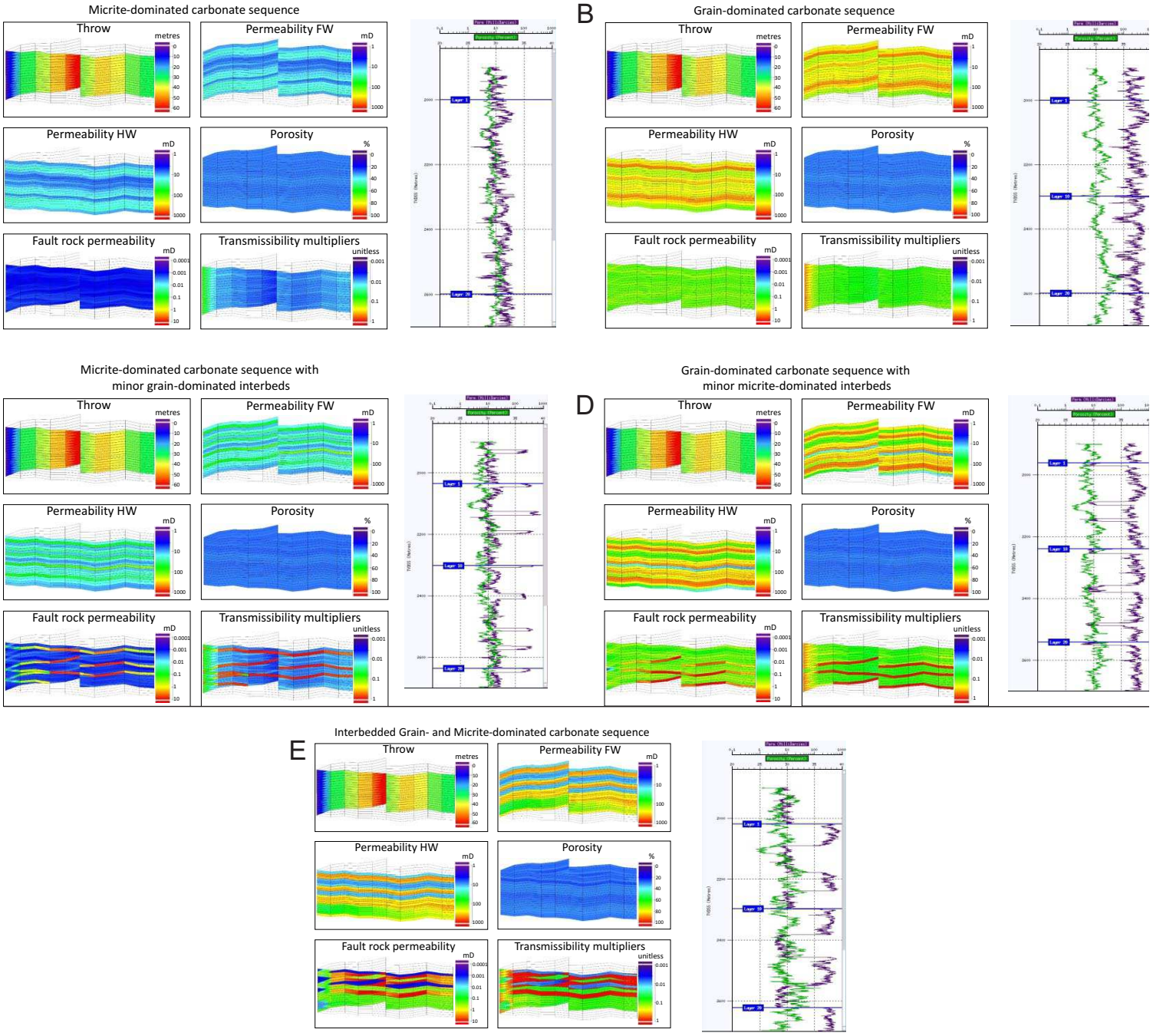
Micrite-dominated carbonate sequence
Throw
metres
Permeability FW
mD
Permeability HW
mD
Porosity
%
Fault rock permeability
mD
Transmissibility multipliers
unitless
B
Grain-dominated carbonate sequence
Throw
metres
Permeability FW
mD
Permeability HW
mD
Porosity
%
Fault rock permeability
mD
Transmissibility multipliers
unitless
Micrite-dominated carbonate sequence with
minor grain-dominated interbeds
Throw
metres
Permeability FW
mD
Permeability HW
mD
Porosity
%
Fault rock permeability
mD
Transmissibility multipliers
unitless
D
Grain-dominated carbonate sequence with
minor micrite-dominated interbeds
Throw
metres
Permeability FW
mD
Permeability HW
mD
Porosity
%
Fault rock permeability
mD
Transmissibility multipliers
unitless
E
Interbedded Grain- and Micrite-dominated carbonate sequence
Throw
metres
Permeability FW
mD
Permeability HW
mD
Porosity
%
Fault rock permeability
mD
Transmissibility multipliers
unitless

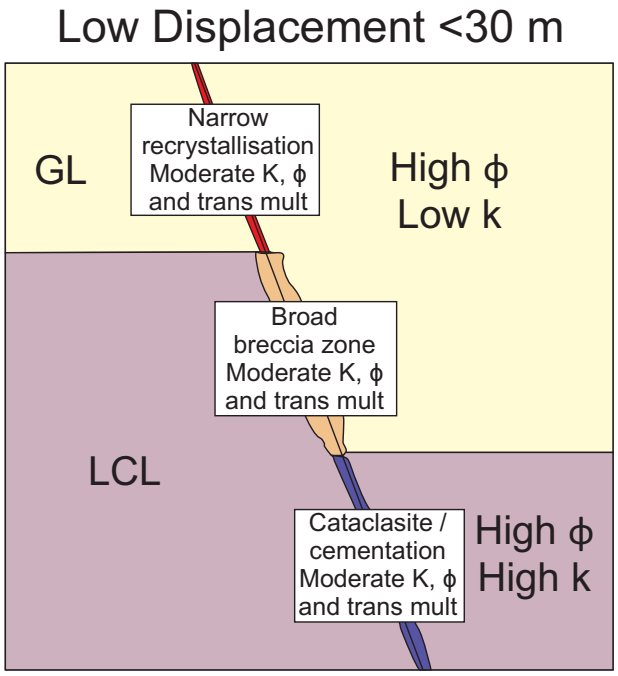
Low Displacement <30 m
GL
Narrow
recrystallisation
Moderate K, ϕ
and trans mult
High ϕ
Low k
Broad
breccia zone
Moderate K, ϕ
and trans mult
LCL
Cataclasite /
cementation
Moderate K, ϕ
and trans mult
High ϕ
High k

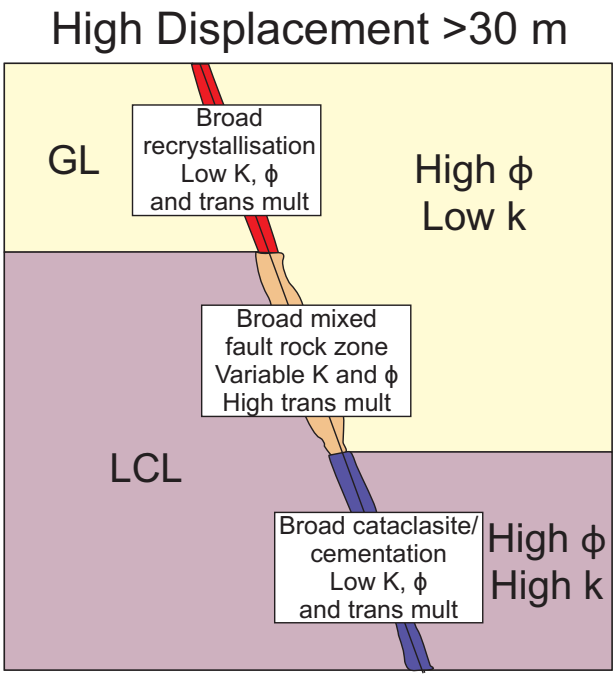
High Displacement >30 m
GL
Broad
recrystallisation
Low K, ϕ
and trans mult
High ϕ
Low k
Broad mixed
fault rock zone
Variable K and ϕ
High trans mult
LCL
Broad cataclasite/
cementation
Low K, ϕ
and trans mult
High ϕ
High k

	Grain-Grain Juxtaposition	**Micrite-Micrite Juxtaposition**	**Grain-Micrite Juxtaposition**
Area weighted harmonic average thickness (m)	0.45	0.44	0.51
Area weighted arithmetic mean permeability (mD)	0.25	0.0021	0.011
Transmissibility (mDm^{-1})	0.37	0.0038	0.01
Transmissibility multiplier	0.3	0.26	0.46

Table 1

	Grain-Grain Juxtaposition	**Micrite-Micrite Juxtaposition**	**Grain-Micrite Juxtaposition**
Area weighted harmonic average thickness (m)	1.77	2.4	1.0
Area weighted arithmetic mean permeability (mD)	0.55	0.0022	6.88
Transmissibility (mDm^{-1})	0.25	0.0009	0.026
Transmissibility multiplier	0.19	0.06	1.0

Table 2